Atomic-layer-deposition alumina induced carbon on porous NixCo1−xO nanonets for enhanced pseudocapacitive and Li-ion storage performance

Guan, Cao; Wang, Yadong; Zacharias, Margit; Wang, John; Fan, Hong Jin

2014

Guan, C., Wang, Y., Zacharias, M., Wang, J., & Fan, H. J. (2015). Atomic-layer-deposition alumina induced carbon on porous NixCo1−xO nanonets for enhanced pseudocapacitive and Li-ion storage performance. Nanotechnology, 26(1), 014001-.

https://hdl.handle.net/10356/81921

https://doi.org/10.1088/0957-4484/26/1/014001

Atomic-layer-deposition Alumina Induced Carbon on Porous $Ni_xCo_{1-x}O$ Nanonets for Enhanced Pseudocapacitive and Li-ion Storage Performance

Cao Guan[1, 2], Yadong Wang[3], Margit Zacharias[4], John Wang[1], and Hong Jin Fan[2]
[1]Department of Materials Science and Engineering, National University of Singapore, 117574 Singapore
E-mail: msewangj@nus.edu.sg
[2]Division of Physics and Applied Physics, School of Physical and Mathematical Sciences, Nanyang Technological University, 637371 Singapore
E-mail: fanhj@ntu.edu.sg
[3]School of Engineering, Nanyang Polytechnic, 569830 Singapore
[4] IMTEK, Faculty of Engineering, Albert-Ludwigs-University Freiburg, Georges-Köhler-Allee 103, 79110 Freiburg, Germany

Keywords: Nanostructures, Energy storage, Atomic layer deposition, Carbon, Metal oxides.

ABSTRACT

A unique composite nanonet of metal oxide@carbon interconnected sheets are obtained by atomic layer deposition (ALD)-assisted fabrication. In this nanonet structure, mesoporous metal oxide nanosheets are covered by a layer of amorphous carbon nanoflakes. Specifically, quasi-vertical aligned and mesoporous $Ni_xCo_{1-x}O$ nanosheets are first fabricated directly on nickel foam substrates by a hydrothermal method. Then an ALD-enabled carbon coating method is applied for the growth of carbon nanoflakes on the surface of the nanosheets. Thus formed 3D hierarchical structure of $Ni_xCo_{1-x}O$@carbon composite flakes have higher surface area, better electric conductivity and structure stability than the bare $Ni_xCo_{1-x}O$. Application of such composite nanomaterials is demonstrated as the electrodes for supercapacitor and lithium-ion battery. In both tests, the composite electrode shows enhancement in capacity and cycling stability. This effective composite nanostructure design of metal oxides@carbon flakes could provide a promising way to the construction of high-performance materials for energy and environment applications.

1. Introduction

Since continuous energy is produced from Sun and wind, together with constant custom demands for better energy storage devices, recent years have witness great research concern on developing high performance electrochemical energy storage devices (such as lithium ion battery and supercapacitor). At nowadays stage, the electrode materials, which act as the most important component in the energy storage devices, are urgently needed to be carefully chosen and designed to accomplish good electrochemical conductivity, high surface area, and high reversible capacity [1-3]. Metal oxides have been widely studied as promising electrodes materials for electrochemical energy storage, owing to the fact that they can offer large energy density (several times higher than that of carbon based materials) by means of various redox reactions [4, 5]. However, metal oxides usually suffered from low electric conductivity, poor ion transport kinetics, and poor cyclic stability [6].

To overcome these shortcomings, an effective way is to fabricate porous and/hollow nanostructured metal oxides [7-9]. The reduced dimensions of the materials will not only increase the electrode/electrolyte interface to provide more reaction cites for higher capacity, but also shorten the ionic and electronic diffusion distance leading to better rate capability [10-14]. On the other hand, the hollow voids can also buffer the strain (generated by fast reaction) and cover the capacity loss (generated with volume change), resulting in better cycling ability [15-17]. In addition, efforts have been made to directly grow metal oxides on conductive substrate, especially nanostructured current collectors [18, 19]. In the light of this, high rate performance can be ensured with reduced resistance for ion diffusion and charge transfer, and improved cycling ability will be achieved with good mechanical adhesion [20-22]. Another useful way is to improve the metal oxides properties by introducing other functionalities, such as high conductivity, high capacity and high surface area, from other active materials (metal oxides, conducting polymers or carbonaceous materials) [23-27]. Typically, doping, surface coating and constructing core-shell (or branched) architectures have been demonstrated to be helpful in obtaining better electrochemical performance [28-32]. For example, surface coating of conductive materials on metal oxide can result in both increased capacitance and better cycling stability [33, 34].

Herein, we report the design and fabrication of a unique 3D nanostructure of metal oxide@carbon flakes, as schematically illustrated in **Figure 1**. Firstly, we intend to fabricate ternary oxides rather than pure CoO, as this has been reported an effective route in increasing both the conductivity and capacity [35-38]. Secondly, by the coating of carbon flakes tangled within the continuous metal oxide skeleton, we aim to further improve the structural stability of the porous oxides by providing connections betwen the skeleton. The carbon shell is obtained exclusively using an ALD-based technique that we elaborated previously [34]. The carbon effectivley increases the overall porosity and structure robustness, and can also contribute extra capacity. Because of the ALD, the obtained carbon coverage is unifromly on any exposed surfaces of the oxide skeleton. Based on these advantageous features, we demonstrate the enhanced properties of the $Ni_xCo_{1-x}O$@f-C composite electrodes for both supercapacitor and lithium-ion storage.

2. Experimental section

2.1. Material synthesis

The hierarchical 3D electrode material was prepared by a three-step process. Firstly, the $Ni_xCo_{1-x}O$ nanonets were synthesized on nickel foam by a hydrothermal process. In detail, nickel foam (20 × 25 × 0.1 mm^3, 100 PPI, 330 g m^{-2}, Changsha Lyrun Material Co., Ltd. China) was pretreated with concentrated HCl solution, absolute ethanol and deionized water for 5 min respectively to ensure its surface was well cleaned. Then the nickel foam with a part leaved as supporting electrode for testing was put in a Teflon-lined stainless steel autoclave with a 50 mL homogeneous solution containing 2.5 mmol $Co(NO_3)_2{\cdot}6H_2O$, 2.5 mmol $Ni(NO_3)_2{\cdot}6H_2O$ and 10 mmol HMT (hexamethylene tetramine). After 8 h growth at 95 ºC, the as-prepared precursors were annealed under a constant flow of argon (50 sccm) at 450 ºC for 2 h. Secondly, the nickel foam with the starting material of $Ni_xCo_{1-x}O$ nanonets was coated with Al_2O_3 with 80 cycles by ALD (Beneq, TFS 200) at 120˚C. Trimethylaluminum [$Al(CH_3)_3$] and water were used as the aluminum and oxygen source, respectively. The thickness of Al_2O_3 is ~10 nm. Finally, the Al_2O_3 coated structures were immersed in 0.04 M glucose for 24 h and annealed in Ar (50 SCCM) at 450 ˚C for 2 h. The Al_2O_3 was removed before the electrochemical test in 1M KOH.

2.2. Characterization

Samples were characterized using scanning electron microscopy (SEM, JSM-6700F, 10.0 kV), transmission electron microscopy (TEM, JEM-2010FEF, 200 kV), X-

ray photoelectron spectroscopy (XPS, PHI 5700), and Raman spectroscopy (WITeck CRM200 confocal microscopy Raman system with a 532 nm laser as excitation light). The mass of electrode materials was measured on an AX/MX/UMX Balance (METTLER TOLEDO, maximum=5.1 g; delta= 0.001 mg). Nitrogen adsorption/desorption isotherms were measured on a Micromeritics TriStar 3000 porosimeter (mesoporous characterization) and Micromeritics ASAP 2020 (microporous characterization) at 77 K. All samples were outgassed at 100 ˚C for 6 h under vacuum before measurements were recorded. The specific surface areas were calculated using the Brunauer-Emmett-Teller (BET) method.

2.3. Electrochemistry measurement

Supercapacitor test: Electrochemical measurements using a workstation (CHI 760D) were performed in a three-electrode electrochemical cell at room temperature using 2 M KOH as the electrolyte. The nickel foam supported nanostructures (~1 cm^2 area; $Ni_xCo_{1-x}O$ mass: ~1.8 mg cm^{-2}; $Ni_xCo_{1-x}O$@f-C mass: ~2.5 mg cm^{-2}) were used directly as the working electrode. A Pt plate and Hg/HgO were used as the counter electrode and reference electrode, respectively. All potentials were referred to the reference electrode. The weight in specific capacitance (F/g) and current rate (A/g) was calculated based on the whole mass of the active materials ($Ni_xCo_{1-x}O$ and carbon), and the small contribution from the Ni foam was subtracted. The specific capacitance was calculated by $C=It/m\Delta V$ and the areal capacitance is calculated by: $C_a=I\cdot t/(\Delta V\cdot S)$, where I is the discharge current, t is the discharge time, m is the mass of the active materials, ΔV is the voltage drop upon discharging, and S is the geometrical area of the electrode.

Lithium ion battery test: Electrochemical measurements were performed using two-electrode CR2032 (3 V) coin-type cells with lithium foil serving as both counter and reference electrodes under ambient temperature. The electrolyte was 1 M LiPF6 in a 50: 50 (w/w) mixture of ethylene carbonate (EC) and dimethyl carbonate (DMC). Cell assembly was carried out in an argon-filled glovebox with both moisture and oxygen contents below 1.0 ppm. Galvanostatic charge/discharge tests were performed using a NEWARE battery tester at a voltage window of 0.005–3 V. Cyclic voltammetry (CV, 0.005–3 V, 0.5 mV s^{-1}) was performed using an electrochemical workstation (CHI 760D).

3. Result and Discussion

3.1. Fabrication and characterization of metal oxides@carbon flakes

The $Ni_xCo_{1-x}O$ nanonets was fabricated with a modified hydrothermal method [39]. From SEM image in Figure 2a, one see that the nanonets covers the nickel foam surfaces uniformly and they are composed of cross linked and vertical aligned nanosheels, each of 2–3 μm in overall size. A large scale view of the nanonets on nickel foam can be found from Figure S1. The higher-magnified SEM image (Figure 2b) and TEM image (Figure 2c) show more clearly the nanonets are indeed composed of small interconnected and porous nanosheets. The pore size ranges from 20 to 50 nm. This porous cross-linked feature is favorable for electrochemical energy storage application as it can provide high active surface areas for electrochemical reaction. To construct the shell structure of carbon flakes, the nanonets are firstly coated with Al_2O_3 by ALD, and then immersed in glucose solution to form a composite layer, following the procedure in our previous report [34]. The microstructure after ALD of Al_2O_3 is shown in Figure S1. After thermal annealing, the core-shell structure was obtained, as schematically illustrated in Figure 1b and by SEM and TEM images in Figure 2d-f. From the low-magnification SEM image in Figure 2d, one can see the overall nanonet structure is fully maintained after the carbon coating. Higher-magnification SEM image (Figure 2e) and TEM image (Figure 2f) reveal that the $Ni_xCo_{1-x}O$ nanonets are embedded with large (width up to 100 nm) carbon nanoflakes, which are also interlinked with each other. It was found that the carbon flakes are generated from an Al_2O_3/glucose composite layer, as elaborated previously. [34] As the starting ALD Al_2O_3 is uniformly coated on the $Ni_xCo_{1-x}O$ skeleton, the resulting carbon nanoflakes after glucose decomposition fully cover the entire surfaces of the metal oxide. As a result, the porous nanonets not only have a better utilization of the open space of the porous skeleton with larger surface areas, but also better electric conductivity and mechanical flexibility.

The 3D $Ni_xCo_{1-x}O$@f-C is further characterized by high-resolution TEM (HRTEM), and result is shown in **Figure 3**. The crystalline structure of the metal oxide can be resolved with lattice distances of 0.15 and 0.24 nm, which are very close to the interplanar spacings of (220) and (111) of $Ni_{0.5}Co_{0.5}O$ (JPCD3984). Figure 3c shows an enlarged image of the carbon nanoflakes, which confirms the porous feature.

The unique core-shell design can also contribute to increased surface area, as confirmed with Brunauer–

Emmett–Teller (BET) method. Figure S2a-b illustrate the nitrogen isotherm adsorption–desorption curves of $Ni_xCo_{1-x}O$ and $Ni_xCo_{1-x}O$@f-C. The surface area of $Ni_xCo_{1-x}O$@f-C determined by BET method is 247.9 m^2 g^{-1}, which is much larger than that of the bare $Ni_xCo_{1-x}O$ (70.5 m^2 g^{-1}), and also larger than that of a reported CoO/reduce graphene oxide composite [40] and a nickel cobaltite/carbon aerogel composites [37]. The increased surface area should stem from the unique core-shell with improved porosity. X-ray photoelectron spectroscopy and Raman spectroscopy have also been carried out to analyze the $Ni_xCo_{1-x}O$ and $Ni_xCo_{1-x}O$@f-C, as shown in **Figure 4**. The Co 2p XPS spectrum shows the two peaks due to Co 2p 3/2 and 2p ½, located at 780.2 and 796.2 eV, respectively. The result is in good agreement with previous report of Co^{2+} [41, 42]. The Ni 2p XPS spectrum shows the Ni 2p 3/2 peak at 854.8eV, which corresponds well with the reported Ni^{2+} [42]. The principal peak of O 1s locates approximately at 529.8 eV, which can be well ascribed to the metal oxide form (O^{2-}) [42]. Based on the XPS spectrum, the atomic ratio of Co:Ni is 1.13:1 (close to the ratio of 1:1 in precursor); and both Co and Ni are in the divalent state, so we can define the material to be $Ni_{0.47}Co_{0.53}O$@f-C. Raman spectroscopy in Figure S2c also shows the composition information of $Ni_xCo_{1-x}O$ and $Ni_xCo_{1-x}O$@f-C. The peaks in the range of 400–700 cm^{-1} corresponds to the Co–O and Ni–O vibrations [23], and they do not obviously change after the carbon coating. The peaks at ~1591 and 1363 cm^{-1} correspond to the G band and D band of carbon, respectively).

3.2. Energy storage properties as supercapacitor electrode

The $Ni_xCo_{1-x}O$ and $Ni_xCo_{1-x}O$@f-C were firstly tested as supercapacitor electrodes. **Figure 5**a illustrates the cyclic voltammetry (CV) curves for the two electrodes measured at a scan rate of 10 mV/s. The redox peaks (and plateau in the discharge curves, see below) is an indication of the pseudocapacitive behavior of the $Ni_xCo_{1-x}O$ ($CoO + OH^- \leftrightarrow CoOOH + e^-$, and $NiO + OH^- \leftrightarrow NiOOH + e^-$). Apparently the enclosed area of the CV curve is dramatically enlarged after the carbon coating. Figure 5b depicts the charge-discharge behavior of the $Ni_xCo_{1-x}O$ and $Ni_xCo_{1-x}O$@f-C electrodes at a same current density of 10 mA cm^{-2}. From the comparison of the two curves, increased capacitance after the carbon coating is further confirmed. The specific capacitance and areal capacitance of the $Ni_xCo_{1-x}O$@f-C is calculated to be about 1077.6 F g^{-1} and 2.69 F cm^{-2}, which is larger than those of the pure $Ni_xCo_{1-x}O$ nanonet electrode (about 551.2 F g^{-1} and 1.06 F cm^{-2}, respectively). The increased capacitance could originate from a better utilization of the metal oxide due to the carbon shell (because of improved conductivity and enhanced surface area enabled), and additional contribution due to electric double layer capacitance. For metal oxides, increasing the charge-discharge rate will usually lead to decreased capacitance due to inadequate reactions [43, 44]. For the $Ni_xCo_{1-x}O$ nanonet, when the current density increases from 5 to 40 mA cm^{-2}, a capacitance retention of 66.1% is achieved (see Figure 5c). And for the 3D $Ni_xCo_{1-x}O$@f-C, the capacitance retention is even higher (70.1%). Furthermore, excellent cycling stability is also observed from the two electrodes, as shown in Figure 5d. The porous $Ni_xCo_{1-x}O$ nanonet maintains 90.9% of its initial capacitance after 10 000 cycles at 10 mA cm^{-2}. Interestingly, the capacitance of the $Ni_xCo_{1-x}O$@f-C is gradually increased after ~1000 cycles and achieves a 110.6% of its initial capacitance after 10 000 cycles at a higher current density of 15 mA cm^{-2}. The increased value may result from the in-depth activation of the porous electrode in the charge-discharge process [45]. In all, the 3D metal oxides@carbon flakes demonstrated high capacitance, good rate capability and excellent durability, which is promising for supercapacitor application.

3.3. Lithium storage property

Application of the composite nanonets in lithium storage has also been investigated. The CV curves of the two materials ($Ni_xCo_{1-x}O$@f-C and $Ni_xCo_{1-x}O$) are firstly recorded to understand the electrochemical reactions, and the first cycles are shown in **Figure 6**a. Both CV curves have two redox peaks which are located at similar positions. For the first discharge cycle of $Ni_xCo_{1-x}O$@f-C, the intense reduction peak at ~0.60 V and a small peak at ~1.28 V correspond to the partially reduction of CoO/NiO to metallic Co/Ni ($CoO + 2Li^+ + 2e^- \leftrightarrow Li_2O + Co$, $NiO + 2Li^+ + 2e^- \leftrightarrow Li_2O + Ni$) and the formation of the solid electrolyte interphase (SEI) film which results in irreversible capacity loss.[37, 46, 47] And the oxidation peak located at ~1.72 V can be attributed to the partially decomposition of SEI, and the peak at ~2.48 V corresponds to the decomposition of Li_2O and metals were converted back to oxides [35]. For pure $Ni_xCo_{1-x}O$, the cathodic peaks shift lower to 0.54 and 1.05 V and the anodic peaks shift higher to 1.78 and 2.66 V, respectively. It is noted that the intensity of cathodic peaks at ~0.6 V and anodic peak locating at ~1.72V of

$Ni_xCo_{1-x}O$@f-C are much higher than those of pure $Ni_xCo_{1-x}O$. This indicates better ionic and electronic conductivity of $Ni_xCo_{1-x}O$@f-C, both can facilitate the charge transfer in electrolyte and promote the decomposition of SEI on the electrodes.[46]

It can be inferred from above C-V result that the carbon shell has improved the ionic and electronic conductivity, therefore providing better electrode utilization and better reaction kinetics. As a result, it would expect to achieve higher lithium ion storage capacity.

Figure S4c-d shows the charge/discharge curves of the two electrodes at a current density of 400 mA g^{-1} from 3.0 to 0.005 V. For pure $Ni_xCo_{1-x}O$ and $Ni_xCo_{1-x}O$@f-C, the initial discharge capacities are 1400 and 1663 mAh g^{-1}, both of which are much higher than the theoretical value (716 mAh g^{-1} for CoO and 718 mAh g^{-1} for NiO). The higher capacity could be attributed to the formation of SEI at the first discharge process, which have been reported on cobalt and nickel based oxides.[48-50]

Figure 6b shows the rate performance of the two electrodes at different current densities from 400 to 2400 mA g^{-1}. One can see obviously that the $Ni_xCo_{1-x}O$@f-C electrode can consistently retain higher capacities than the pure $Ni_xCo_{1-x}O$ electrode when the current density varies from 400 to 2400 mA g^{-1} and back to 400 mA g^{-1}. Also, the initial Columbic efficiency of the former electrode is 73.0% compared to 69.0% of the later. The improved rate capability can be attributed to the fact that the carbon flake shell can buffer the strain at high rates and maintain kinetics with facile charge transport.[51]

To further illustrate the merits of the composite nanonet structure, electrochemical impedance spectroscopy (EIS) and cycling stability were tested. Figure 6c shows the Nyquist plots of the two electrodes. In the high frequency region, the intercepts with the real impedance axis represents the ohmic resistance between the electrode and electrolyte. The $Ni_xCo_{1-x}O$@f-C sample has a much smaller bulk resistance than the pure $Ni_xCo_{1-x}O$. This may be due to the carbon shell that increases the contact area between the electrode and the electrolyte. The diameter of the semicircle corresponds to the charge transfer resistance between the electrode and electrolyte and the slope of the curve in the low frequency region reflects the diffusion resistance of the ions into the electrode, One can see that the $Ni_xCo_{1-x}O$@f-C also demonstrates better electrochemical properties for charge transfer and ion diffusion, in accordance to their improved charge storage properties from the C-V and discharge curves.

Finally, as an important feature for lithium ion battery, the cycling abilities of both electrode materials are also tested, as shown in Figure 6d. One major reason to the usually observed capacity degradation for metal oxide electrode is the structural deterioration and/or detachment from the current collector. This is caused by mechanical stress generated from volume expansion/contraction during the repeated lithiation and delithiation process. Figure 6d shows that, at a current density of 400 mA g^{-1}, the $Ni_xCo_{1-x}O$@f-C can maintain a stable capacity of 1093.5 mA h g^{-1} after 50 cycles, while the capacity of $Ni_xCo_{1-x}O$ after 50 cycles is only 536.0 mA h g^{-1}. The improved cycling stability can be attributed also to the carbon nanoflakes that can effectively buffer the mechanical stress and provide a linkage between individual $Ni_xCo_{1-x}O$ nanocrystallites.

The low-temperature ALD Al_2O_3 is the key to the formation of carbon shells through the formation of an Al_2O_3-glucose composite layer. Such flake carbon provides a soft buffer for the oxides network in the lithium-ion storage, and more surface areas in the suprecapacitors. For both devices, a lowering of the impedance also contributes to the improved electrochemical energy storage property. On the other hand, prospectively, a direct carbon coating by molecular layer deposition (MLD) would also be a feasible and good choice for LIB electrodes.[52, 53]

4. Conclusions

A novel 3D nanonet structure of ternary metal oxide nanonets@carbon flakes has been successfully fabricated. Networks of porous $Ni_xCo_{1-x}O$ sheets were coated and wrapped with continuous carbon flakes with assistance of ALD. The resulting material can be utilized as mechanically robust and electrochemical conductive electrode with high surface areas. As demonstrated, such composite electrodes exhibit high specific capacitance and excellent cycling ability in supercapacitor test, and also high lithium storage capacity with good cycling stability, as compared to bare oxides without carbon coating. Our strategy for the construction of carbon flakes on ternary metal oxides can be easily extended to the rational design of many other systems for various electrochemical energy applications.

Acknowledgement

This research is supported by the joint Singaporean-German Research Projects (SGP-PROG-021) and also funded by SERC Public Sector Research Funding (Grant number 1121202012), Agency for Science, Technology,

and Research (A*STAR). We thank Dr. Zeng Zhiyuan for the help with battery assembly.

Reference

[1] Wang G, Zhang L and Zhang J 2012 A review of electrode materials for electrochemical supercapacitors *Chem. Soc. Rev*. **41** 797-828

[2] Cheng C and Fan H J 2012 Branched nanowires: Synthesis and energy applications *Nano Today* **7** 327-43

[3] Mukherjee R, Krishnan R, Lu T-M and Koratkar N 2012 Nanostructured electrodes for high-power lithium ion batteries *Nano Energy* **1** 518-33

[4] Jiang J, Li Y, Liu J, Huang X, Yuan C and Lou X W 2012 Recent Advances in Metal Oxide-based Electrode Architecture Design for Electrochemical Energy Storage *Adv. Mater.* **24** 5166-80

[5] Ban C, Xie M, Sun X, Travis J J, Wang G, Sun H, Dillon A C, Lian J and George S M 2013 Atomic layer deposition of amorphous TiO 2 on graphene as an anode for Li-ion batteries *Nanotechnology* **24** 424002

[6] Wang H and Dai H 2013 Strongly coupled inorganic-nano-carbon hybrid materials for energy storage *Chem. Soc. Rev.* **42** 3088-113

[7] Cho W, Lee Y H, Lee H J and Oh M 2011 Multi Ball-In-Ball Hybrid Metal Oxides *Adv. Mater.* **23** 1720-3

[8] Shao M, Ning F, Zhao Y, Zhao J, Wei M, Evans D G and Duan X 2012 Core–Shell Layered Double Hydroxide Microspheres with Tunable Interior Architecture for Supercapacitors *Chem. Mater.* **24** 1192-7

[9] Liu J, Xia H, Xue D and Lu L 2009 _Double-Shelled Nanocapsules of V2O5-Based Composites as High-Performance Anode and Cathode Materials for Li Ion Batteries *Journal of the American Chemical Society* **131** 12086-7

[10] Xiao Y, Liu S, Li F, Zhang A, Zhao J, Fang S and Jia D 2012 3D Hierarchical Co3O4 Twin-Spheres with an Urchin-Like Structure: Large-Scale Synthesis, Multistep-Splitting Growth, and Electrochemical Pseudocapacitors *Adv. Funct. Mater.* **22** 4052-9

[11] Lai X, Halpert J E and Wang D 2012 Recent advances in micro-/nano-structured hollow spheres for energy applications: From simple to complex systems *Energy Environ. Sci.* **5** 5604-18

[12] Guan C, Xia X, Meng N, Zeng Z, Cao X, Soci C, Zhang H and Fan H J 2012 Hollow core-shell nanostructure supercapacitor electrodes: gap matters *Energy Environ. Sci.* **5** 9085-90

[13] Zhou C and Liu J 2014 Carbon nanotube network film directly grown on carbon cloth for high-performance solid-state flexible supercapacitors *Nanotechnology* **25** 035402

[14] Zhou R, Meng C, Zhu F, Li Q, Liu C, Fan S and Jiang K 2010 High-performance supercapacitors using a nanoporous current collector made from super-aligned carbon nanotubes *Nanotechnology* **21** 345701

[15] Wu H, Chan G, Choi J W, Ryu I, Yao Y, McDowell M T, Lee S W, Jackson A, Yang Y, Hu L and Cui Y 2012 Stable cycling of double-walled silicon nanotube battery anodes through solid-electrolyte interphase control *Nat Nano* **7** 310-5

[16] Hwang T H, Lee Y M, Kong B-S, Seo J-S and Choi J W 2011 Electrospun Core–Shell Fibers for Robust Silicon Nanoparticle-Based Lithium Ion Battery Anodes *Nano Lett.* **12** 802-7

[17] Zhao Y, Li J, Wu C, Ding Y and Guan L 2012 A Yolk–Shell Fe3O4@C Composite as an Anode Material for High-Rate Lithium Batteries *ChemPlusChem* **77** 748-51

[18] Liu J, Cao G, Yang Z, Wang D, Dubois D, Zhou X, Graff G L, Pederson L R and Zhang J-G 2008 Oriented Nanostructures for Energy Conversion and Storage *ChemSusChem* **1** 676-97

[19] Cao X, Shi Y, Shi W, Lu G, Huang X, Yan Q, Zhang Q and Zhang H 2011 Preparation of Novel 3D Graphene Networks for Supercapacitor Applications *Small* **7** 3163-8

[20] Guan C, Liu J, Cheng C, Li H, Li X, Zhou W, Zhang H and Fan H J 2011 Hybrid structure of cobalt monoxide nanowire @ nickel hydroxidenitrate nanoflake aligned on nickel foam for high-rate supercapacitor *Energy Environ. Sci.* **4** 4496-9

[21] Ha D-H, Islam M A and Robinson R D 2012 Binder-Free and Carbon-Free Nanoparticle Batteries: A Method for Nanoparticle Electrodes without Polymeric Binders or Carbon Black *Nano Lett.* **12** 5122-30

[22] He Y, Chen W, Li X, Zhang Z, Fu J, Zhao C and Xie E 2012 _Freestanding Three-Dimensional Graphene/MnO2 Composite Networks As Ultralight and Flexible Supercapacitor Electrodes *ACS Nano* **7** 174-82

[23] Zhong J-H, Wang A-L, Li G-R, Wang J-W, Ou Y-N and Tong Y-X 2012 Co3O4/Ni(OH)2 composite mesoporous nanosheet networks as a promising electrode for supercapacitor applications *J. Mater. Chem.* **22** 5656-65

[24] Liu Y, Zhang W, Zhu Y, Luo Y, Xu Y, Brown A, Culver J N, Lundgren C A, Xu K, Wang Y and Wang C 2012 Architecturing Hierarchical Function Layers on Self-Assembled Viral Templates as 3D Nano-Array Electrodes for Integrated Li-Ion Microbatteries *Nano Lett.*

[25] Li J, Yang M, Wei J and Zhou Z 2012 Preparation and electrochemical performances of doughnut-like Ni(OH)2-Co(OH)2 composites as pseudocapacitor materials *Nanoscale* **4** 4498-503

[26] Zhou W, Zhu J, Cheng C, Liu J, Yang H, Cong C, Guan C, Jia X, Fan H J, Yan Q, Li C M and Yu T 2011 A general strategy toward graphene@metal oxide core-shell nanostructures for high-performance lithium storage *Energy Environ. Sci.* **4** 4954-61

[27] Chen Y M, Cai J H, Huang Y S, Lee K Y and Tsai D S 2011 Preparation and characterization of iridium dioxide–carbon nanotube nanocomposites for supercapacitors *Nanotechnology* **22** 115706

[28] Pasero D, Reeves N and West A R 2005 Co-doped Mn3O4: a possible anode material for lithium batteries *J. Power Sources* **141** 156-8

[29] Boukhalfa S, Evanoff K and Yushin G 2012 Atomic layer deposition of vanadium oxide on carbon nanotubes for high-power supercapacitor electrodes *Energy Environ. Sci.* **5** 6872-9

[30] Yang L, Wang S, Mao J, Deng J, Gao Q, Tang Y and Schmidt O G 2012 Hierarchical MoS2/Polyaniline Nanowires with Excellent Electrochemical Performance for Lithium-Ion Batteries *Adv. Mater.* **25** 1180-4

[31] Huang F and Chen D 2012 Towards the upper bound of electrochemical performance of ACNT@polyaniline arrays as supercapacitors *Energy Environ. Sci.* **5** 5833-41

[32] Han J, Dou Y, Zhao J, Wei M, Evans D G and Duan X 2012 Flexible CoAl LDH@PEDOT Core/Shell Nanoplatelet Array for High-Performance Energy Storage *Small* **9** 98-106

[33] Yu G, Hu L, Liu N, Wang H, Vosgueritchian M, Yang Y, Cui Y and Bao Z 2011 Enhancing the Supercapacitor Performance of Graphene/MnO2 Nanostructured Electrodes by Conductive Wrapping *Nano Lett.* **11** 4438-42

[34] Guan C, Zeng Z, Li X, Cao X, Fan Y, Xia X, Pan G, Zhang H and Fan H J 2014 Atomic-Layer-Deposition-Assisted Formation of Carbon Nanoflakes on Metal Oxides and Energy Storage Application *Small* **10** 300-7

[35] NuLi Y, Zhang P, Guo Z, Liu H, Yang J and Wang J 2009 Nickel–cobalt oxides/carbon nanoflakes as anode materials for lithium-ion batteries *Mater. Res. Bull.* **44** 140-5

[36] Yang F, Yao J, Liu F, He H, Zhou M, Xiao P and Zhang Y 2013 Ni-Co oxides nanowire arrays grown on ordered TiO2 nanotubes with high performance in supercapacitors *J. Mater. Chem. A* **1** 594-601

[37] Chien H-C, Cheng W-Y, Wang Y-H and Lu S-Y 2012 Ultrahigh Specific Capacitances for Supercapacitors

Achieved by Nickel Cobaltite/Carbon Aerogel Composites *Adv. Funct. Mater.* **22** 5038-43
[38] Wang H, Gao Q and Jiang L 2011 Facile Approach to Prepare Nickel Cobaltite Nanowire Materials for Supercapacitors *Small* **7** 2454-9
[39] Guan C, Li X, Wang Z, Cao X, Soci C, Zhang H and Fan H J 2012 Nanoporous Walls on Macroporous Foam: Rational Design of Electrodes to Push Areal Pseudocapacitance *Adv. Mater.* **24** 4186-90
[40] Zhu J, Sharma Y K, Zeng Z, Zhang X, Srinivasan M, Mhaisalkar S, Zhang H, Hng H H and Yan Q 2011 Cobalt Oxide Nanowall Arrays on Reduced Graphene Oxide Sheets with Controlled Phase, Grain Size, and Porosity for Li-Ion Battery Electrodes *J. Phys. Chem. C* **115** 8400-6
[41] Hassel M and Freund H-J 1996 High Resolution XPS Study of a Thin CoO(111) Film Grown on Co(0001) *Surf. Sci. Spectra* **4** 273-8
[42] Nydegger M W, Couderc G and Langell M A 1999 Surface composition of CoxNi1−xO solid solutions by X-ray photoelectron and Auger spectroscopies *Appl. Surf. Sci.* **147** 58-66
[43] Zhao X, Sanchez B M, Dobson P J and Grant P S 2011 The role of nanomaterials in redox-based supercapacitors for next generation energy storage devices *Nanoscale* **3** 839-55
[44] Lu Z, Zhu W, Lei X, Williams G R, O'Hare D, Chang Z, Sun X and Duan X 2012 High pseudocapacitive cobalt carbonate hydroxide films derived from CoAl layered double hydroxides *Nanoscale* **4** 3640-3
[45] Dong X-C, Xu H, Wang X-W, Huang Y-X, Chan-Park M B, Zhang H, Wang L-H, Huang W and Chen P 2012 3D Graphene–Cobalt Oxide Electrode for High-Performance Supercapacitor and Enzymeless Glucose Detection *ACS Nano* **6** 3206-13
[46] Mai Y J, Tu J P, Xia X H, Gu C D and Wang X L 2011 Co-doped NiO nanoflake arrays toward superior anode materials for lithium ion batteries *J. Power Sources* **196** 6388-93
[47] Wang X, Li X, Sun X, Li F, Liu Q, Wang Q and He D 2011 Nanostructured NiO electrode for high rate Li-ion batteries *J. Mater. Chem.* **21** 3571-3
[48] Wang Y, Zhang H J, Lu L, Stubbs L P, Wong C C and Lin J 2010 Designed Functional Systems from Peapod-like Co@Carbon to Co3O4@Carbon Nanocomposites *ACS Nano* **4** 4753-61
[49] Wang B, Cheng J L, Wu Y P, Wang D and He D N 2012 Porous NiO fibers prepared by electrospinning as high performance anode materials for lithium ion batteries *Electrochem. Commun.* **23** 5-8
[50] Li Y, Tan B and Wu Y 2007 Mesoporous Co3O4 Nanowire Arrays for Lithium Ion Batteries with High Capacity and Rate Capability *Nano Lett.* **8** 265-70
[51] Gu Y, Wu F and Wang Y 2012 Confined Volume Change in Sn-Co-C Ternary Tube-in-Tube Composites for High-Capacity and Long-Life Lithium Storage *Adv. Funct. Mater.* **23** 893-9
[52] Yang P, Wang G, Gao Z, Chen H, Wang Y and Qin Y 2013 Uniform and Conformal Carbon Nanofilms Produced Based on Molecular Layer Deposition *Materials* **6** 5602-12
[53] Tong X, Yang P, Wang Y, Qin Y and Guo X 2014 Enhanced photoelectrochemical water splitting performance of TiO2 nanotube arrays coated with an ultrathin nitrogen-doped carbon film by molecular layer deposition *Nanoscale* **6** 6692-700

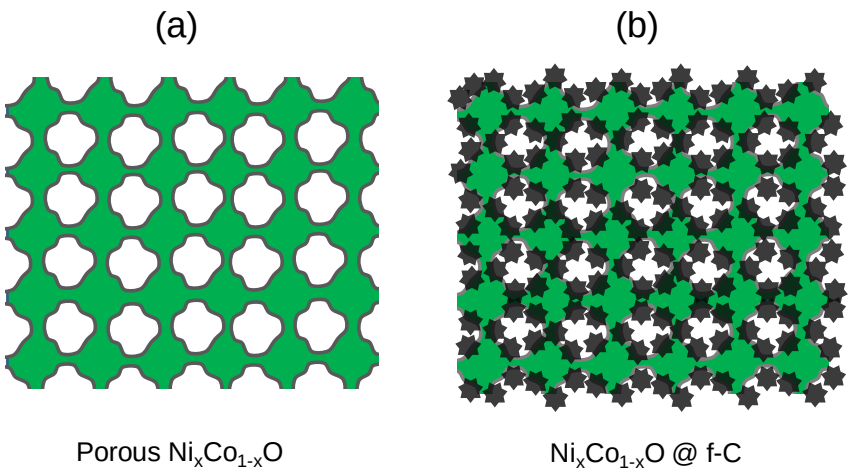

Figure 1. Schematics of the nanostructure. (a) As-grown $Ni_xCo_{1-x}O$ porous sheets. (b) $Ni_xCo_{1-x}O$ @carbon composite sheets after the growth of carbon nanoflakes via ALD alumina assisted carbonization.

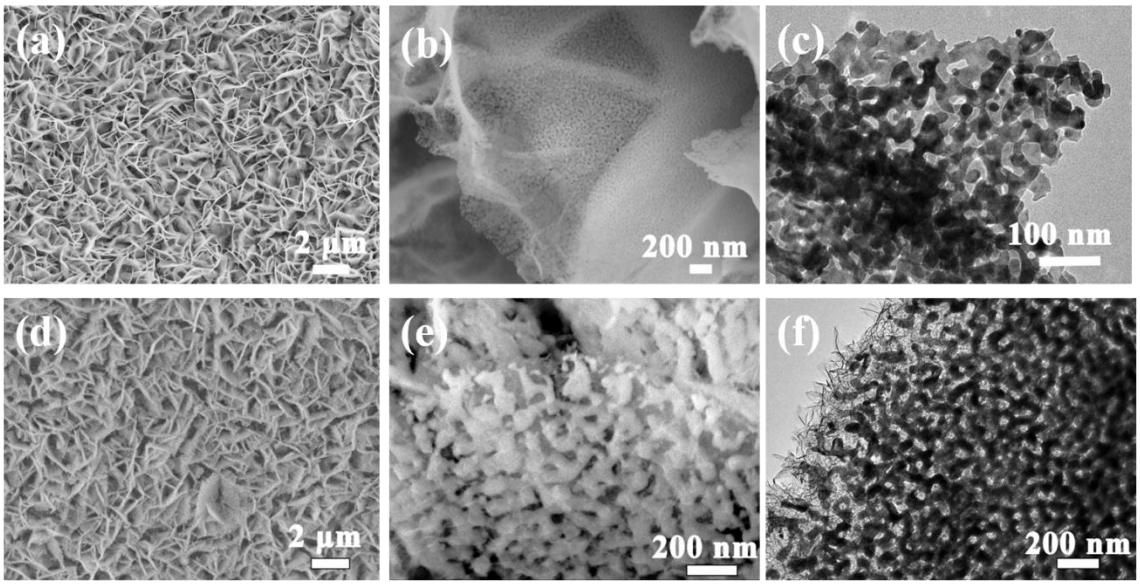

Figure 2. (a-c) SEM and TEM images of the $Ni_xCo_{1-x}O$ nanonet made of interconnected porous sheets. (d-f) SEM and TEM images of $Ni_xCo_{1-x}O$@f-C composite sheets.

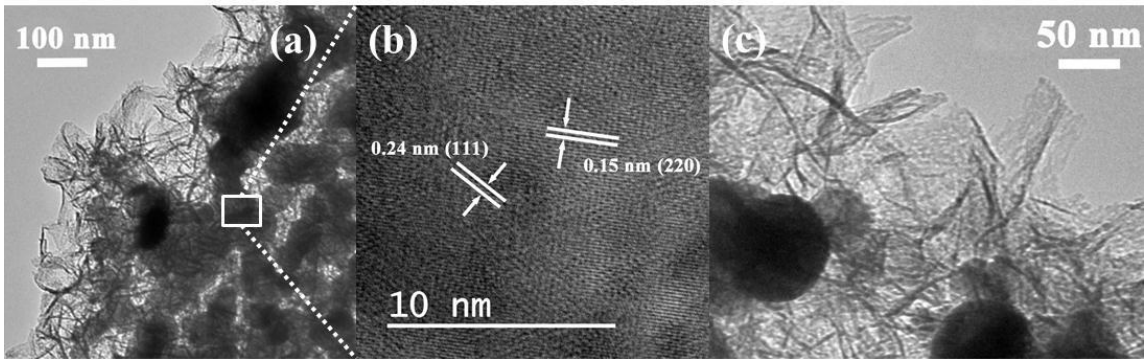

Figure 3. Higher-magnification TEM images of a portion of the $Ni_xCo_{1-x}O$ @Carbon flakes. The carbon has an amorphous and mesoporous structure. HRTEM image of the $Ni_xCo_{1-x}O$ nanocrystallite is shown in (b).

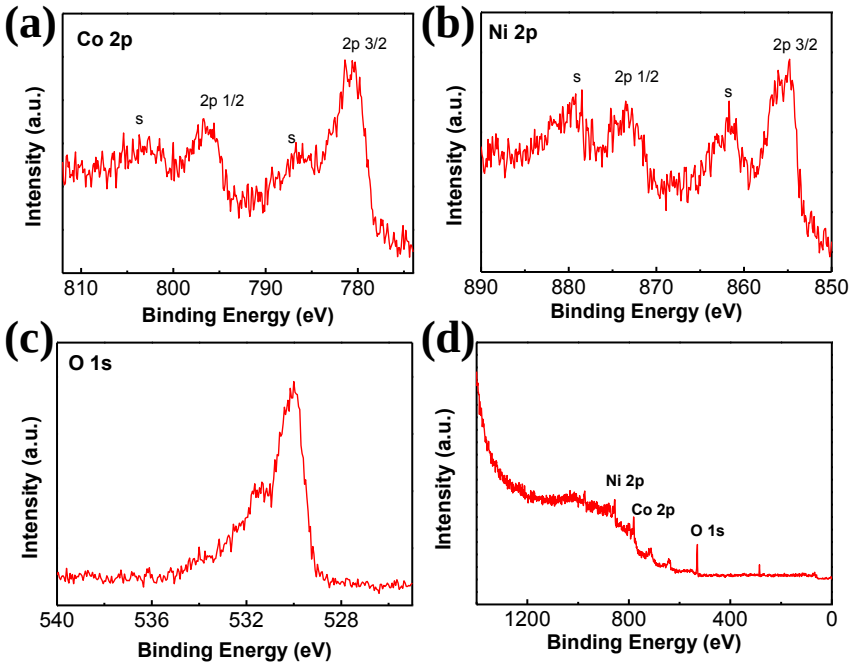

Figure 4. XPS test shows the metal oxide can be defined as $Ni_{0.47}Co_{0.53}O$

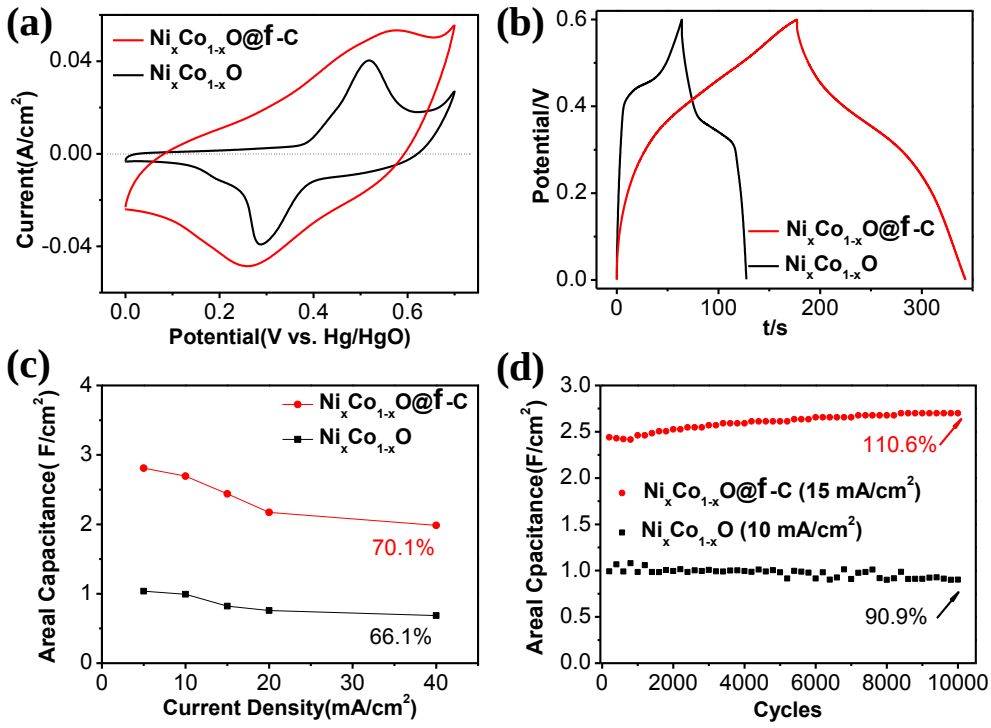

Figure 5. Electrochemical property as supercapacitor electrode. (a) CV and (b) charge-discharge curves of $Ni_xCo_{1-x}O$ and $Ni_xCo_{1-x}O$@f-C electrodes. (c) Rate capability and (d) Cycling stability of $Ni_xCo_{1-x}O$ and $Ni_xCo_{1-x}O$@f-C. The percentage numbers in (c) denote the capacitance retention when the current is increased from 5 to 40 mA cm^{-2}, and the ones in (d) denote the capacitance retention after 10 000 cycles of charge–discharge.

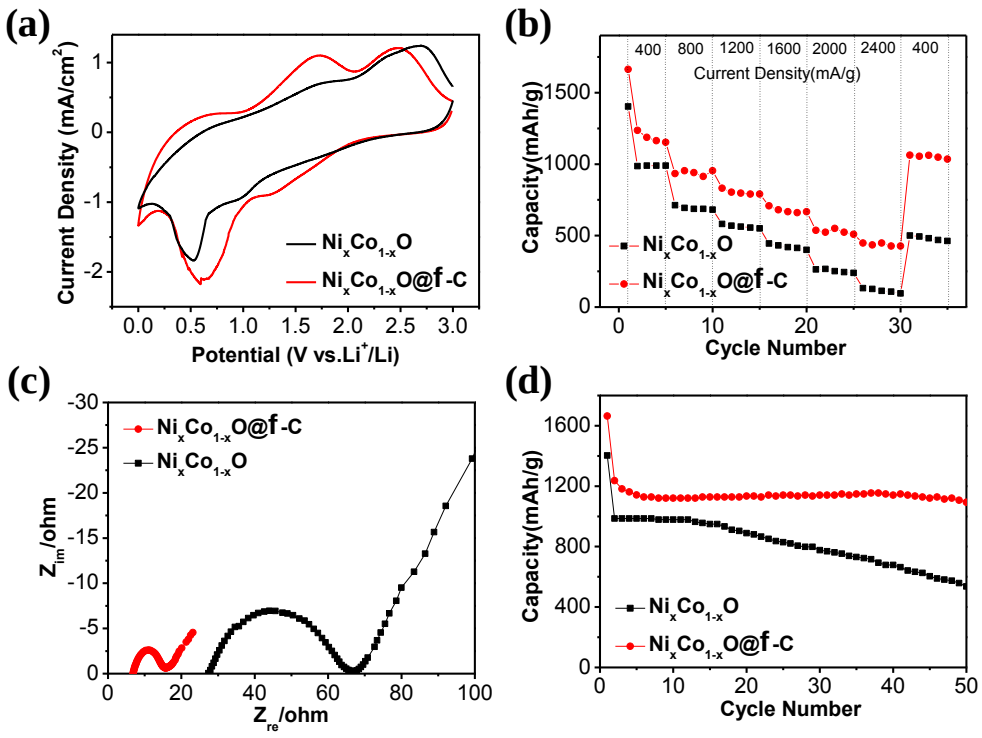

Figure 6. Electrochemical property as lithium ion battery anode. (a) CV curves of the first cycle for $Ni_xCo_{1-x}O$ and $Ni_xCo_{1-x}O$@f-C. (b) Rate capability, (c) Electrochemical Impedance Spectroscopy, and (d) cycling stability of the two materials.